

**Best
Available
Copy**

②

17. Under response, including the time for reviewing instructions, searching existing data sources, gathering of information, sending comments regarding this burden estimate or any other aspect of this collection of information, Send comments regarding this burden estimate or any other aspect of this collection of information, including suggestions for reducing this burden, to Washington Headquarters Services, Directorate for Information Operations and Reports, 1215 Jefferson Davis Highway, Suite 1204, Arlington, VA 22202-4302, and to the Office of Management and Budget, Paperwork Reduction Project (0304-0138), Washington, DC 20503.

Standard Form 298 (Rev. 2-89)
Prescribed by ANSI Std. Z39-18
298-102

CONSEQUENCES OF CHROMOSPHERIC IRRADIATION IN WHITE LIGHT FLARES: AN OBSERVER'S POINT OF VIEW

D. F. Neidig

*Phillips Laboratory (AFMC), Geophysics Directorate, National Solar
 Observatory/Sacramento Peak, National Optical Astronomy Observatories,
 Sunspot, NM 88349, U.S.A.*

ABSTRACT

Irradiation of the photosphere by chromospheric flare continuum has been suggested as a mechanism of energy transport in white light flares. In this model the flare optical continuum originates from both the chromosphere (H_{β} emission) and the photosphere (H^{-} emission). Consequences of the irradiation model include different dependences on viewing angle of the two continuum components and reduction in minimum required chromospheric energy deposition rate, for a given visible light flare intensity, relative to models which assume only a chromospheric source. Testable predictions of the irradiation model, relating to specific effects on spatial variation and timing of flare emissions, are discussed.

INTRODUCTION

Irradiation of the solar photosphere by intense visible and near UV chromospheric continua has been previously suggested as an energy transport mechanism in white light flares (WLFs) /1,2/. One motivation for considering this process is that the radiative output in chromospheric hydrogen recombination (H_{β}) continua can be quite large in the case of WLFs /3,4/; and, because half of the total chromospheric output must be radiated downward, it will be absorbed at atmospheric depths approximately where optical depth unity is achieved, i.e., the photosphere. A second motivation is that spectrographic observations of WLFs have provided evidence for the presence of both chromospheric and photospheric components /3,4,5,6/. Yet various energy transport mechanisms suggested previously have not proven effective in heating the photospheric layers to a sufficient degree to account for WLFs /4/; thus some other mechanism, which is efficient at relatively large depth in the atmosphere, is required. High energy electron beams, long favored as an energy transport mechanism in the flare impulsive phase, do not carry sufficient power (by a factor $\geq 10^2$) directly to photospheric levels, although they might be able to balance the WLF radiative losses in the chromosphere /7,8/.

The following sections discuss the salient features of the irradiation model, the major consequences relevant to questions of energy balance and transport, and the spectral and temporal signatures which might be observed, given sufficient spatial and temporal resolution. It is assumed, as a starting point, that a source of strong chromospheric flare emission exists as a result of some initial heating mechanism that is effective at chromospheric depths.

THE IRRADIATION MODEL

The irradiation model is illustrated in Figure 1. A chromospheric flare source (assumed to be a homogeneous slab) with nominal temperature $T_c \approx 10^4$ K, electron density $N_e \approx 5 \times 10^{13} \text{ cm}^{-3}$, and vertical thickness 130 km (one density scale height) produces strong chromospheric H_{β} emission. These assumed conditions correspond to the Balmer components of the largest flares /9/, and of WLFs in particular /3,4/. The chromospheric emission is radiated both upward and downward, with the latter being absorbed in the photosphere where it produces a temperature increase of order 10^2 K /1,2/. Photospheric

94-00271



energy balance is then restored by enhanced radiation by the H^- ion (it is assumed that all of the energy is returned as radiation, i.e., dynamical responses are negligible). The latter emission will be roughly Plankian in form with characteristic temperature near 6000 K.

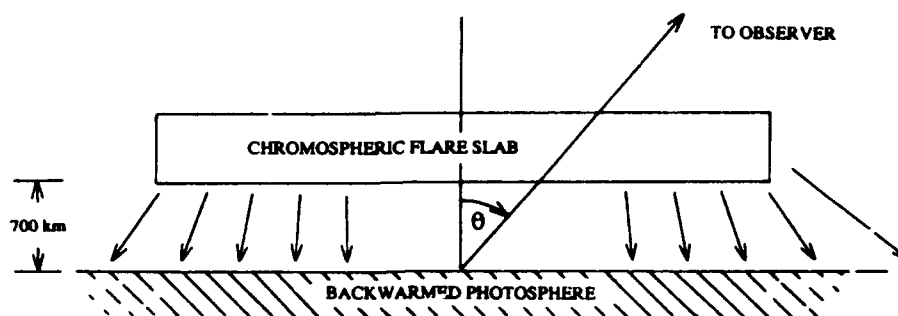


Fig. 1. Schematic representation of WLF irradiation model showing a chromospheric flare source and the resulting backwarmed photosphere (not drawn to scale).

The chromospheric and photospheric flare layers are separated only by about 700 km, so that, if the lateral dimensions of the flare are much larger than 700 km, the downward flux incident on the top of the photosphere, near the center of the flare, will be approximately equal to the flux emitted from the bottom of the chromospheric layer. Using the chromospheric flux derived from the assumed physical conditions above, the elevated photospheric equilibrium temperature can be estimated [8], from which the emergent photospheric spectrum can be calculated. This spectrum, assumed to be a blackbody radiator modified by a standard solar line blanketing function, is included along with the calculated chromospheric spectrum in Figure 2. Near the edge of the flare, the relative spectral intensities of the chromospheric and photospheric components will differ from those given in Figure 2, due to dilution of the chromospheric radiation field at the photospheric level. An important feature of the irradiation model is the effective conversion of Balmer continuum (which contains approximately 2/3 of the chromospheric power, when the chromospheric temperature is 10^4 K) into visible light.

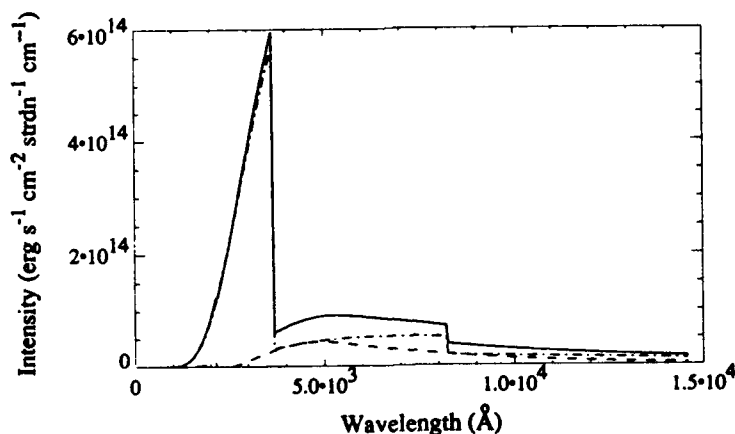


Fig. 2. Calculated WLF spectrum (flare minus background) at the center of the flare, for the chromospheric conditions assumed in the text, at 76° viewing angle. Dash curve: the photospheric component (corresponding to a 300 K increase in photospheric radiation temperature). Dash-dot curve: the chromospheric component (the Lyman continuum is not included in this calculation because, due to the large opacity in Lyman continuum, it is unlikely that the latter radiation could reach the photosphere). Solid curve: the total emergent intensity.

In addition to calculating the flare spectrum, the variation of the emergent intensity at a fixed wavelength as a function of viewing angle θ can, in principle, be determined /8/. For the chromospheric component this is a trivial exercise, as the chromospheric flare slab is nearly optically thin. The photospheric component, however, is subject to self absorption as well as absorption by the ambient quiet atmosphere. Thus we require a knowledge of the "limb darkening" function for the photospheric flare layer, which is not available in models discussed thus far. Herein, it is assumed that the flare limb darkening function is similar to that of the quiet sun. The 5000 Å intensity variations of the chromospheric and photospheric components, as a function of θ , are shown in Figure 3, again using the chromospheric flare conditions assumed above. The ratio of chromospheric to photospheric intensity at any θ , however, is virtually independent of the assumed chromospheric flux, although it is sensitive to the assumed chromospheric flare temperature and photospheric flare limb darkening function. Further details are given elsewhere /8/.

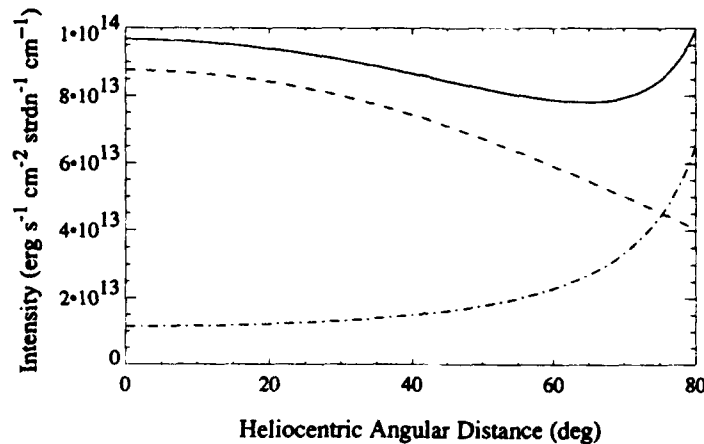


Fig. 3. The 5000 Å continuum intensity (flare minus background) as a function of viewing angle, for the same conditions as in Figure 2. Dash curve: photospheric component. Dash-dot curve: chromospheric component. Solid curve: the total emergent intensity. The curves have been terminated at $\theta = 80^\circ$ due to the breakdown of plane-parallel geometry near the limb.

The results of Figure 3 indicate that the chromospheric source, being nearly optically thin and having lateral dimension much larger than the vertical, produces a steady increase in intensity toward the limb. The photospheric component, which may be subject to limb darkening, shows the opposite trend, so that at $\theta \approx 75^\circ$ the intensity curves at 5000 Å cross over. Note that the spectra of the two flare components shown in Figure 2 have been calculated at a θ -value near this cross-over point.

CONSEQUENCES OF THE IRRADIATION MODEL

The first consequence of the irradiation model, already noted above, is the variation with θ in the relative intensity contributions of the chromospheric and photospheric components. The irradiation model predicts that WLFs observed in visible wavelengths near disk center will be dominated by photospheric emission, those at the limb by chromospheric emission. This effect, which can be sought in future spectrographic analyses of WLFs, constitutes one observational test of the irradiation model.

A second consequence stems from the fundamental feature that the flare chromosphere in the irradiation model produces a smaller intensity contribution at *visible* wavelengths than would be required of models that assume an *entirely* chromospheric origin of the flare emission. For a given observed visible-light continuum intensity, this effectively reduces the required chromospheric energy deposition rate. The reduced chromospheric intensity may further imply a smaller requirement on the chromospheric emission measure, which, if it implies a lower chromospheric density, would then allow the source to be positioned at greater height in the chromosphere. Together, the reduced chromospheric energy deposition rate and the possibly increased source height would significantly enhance the possibility that energetic electrons, for example, might be able to balance the entire radiative losses of the WLF.

A third and more subtle consequence concerns the observed WLF output. Given some viewing angle and observed intensity, the measurement of the radiative output requires an integration of the flare intensity over solid angle, which in turn requires some assumption on the angular distribution of the flare intensity. Figure 3 reminds us that the latter distribution could be quite different for the photospheric and chromospheric components. Furthermore, because the fraction of the total intensity that resides in these two components is strongly dependent on viewing angle, an accurate assessment of the radiative output is not possible without the aid of Figure 3 (or an improved version of it which properly accounts for the photospheric flare limb darkening function), even when the full spectrum is known.

A fourth consequence is the prediction of a delay of possibly several seconds or more in the appearance of the photospheric component relative to the chromospheric continua. The delay would arise as a natural consequence of the heat capacity of the relatively large irradiated photospheric column mass (estimated to be $5 \text{ gm cm}^{-2} / 1$). In observing this delay with spectrographs, careful spectral analysis may be required in order to separate the chromospheric and photospheric components; alternatively, high speed imaging in Balmer continuum (where the emission may be dominated by the chromospheric component) and Paschen continuum might suffice. Observation of such delays, using currently available instrumentation and modeling techniques for spectral interpretation, would provide a second test of the irradiation model.

A fifth consequence of the irradiation model, and constituting a third, although difficult, observational test, is a spatial variation of the flare spectrum that must occur as a result of the spreading of the chromospheric radiation. As noted above, the flux incident on the photosphere will be approximately equal to the emergent chromospheric flux at points near the center of the flare, while toward the flare's edge the chromospheric radiation will be increasingly diluted. Therefore, compared with the chromospheric component, the photospheric component will have a broader spatial distribution, with its largest relative contribution to the total emergent flare intensity occurring near flare center. Further, given sufficient resolution (exceeding 1 arcsec), the approximate 700 km separation of the two flare layers might be detected in spatially resolved spectral signatures of WLFs near the solar limb.

CONCLUSIONS

The irradiation model is attractive because it includes the downward emission of WLF radiation from the chromosphere, and thereby provides a mechanism of energy transport to the underlying photosphere. In doing so, the entire radiative output from the chromosphere (over 4π strdn) is effectively returned to the 2π strdn outward from the Sun, thus offering enhanced prospect for traditional impulsive phase energy transport mechanisms, e.g. energetic electron beams, in balancing the total WLF radiative losses. The model offers several specific predictions which might be testable at the spatial and temporal resolutions of currently available instrumentation.

REFERENCES

1. J. Aboudarham and J. C. Henoux, *Solar Phys.* **121**, 19 (1989).
2. M. E. Machado, A. G. Emslie, and E. H. Avrett, *Solar Phys.* **124**, 303 (1989).
3. D. F. Neidig, *Solar Phys.* **85**, 285 (1983).
4. D. F. Neidig, *Solar Phys.* **121**, 261 (1989).
5. R. Boyer, M. E. Machado, D. M. Rust, and P. Sotirovski, *Solar Phys.* **98**, 255 (1985).
6. P. J. D. Mauas, M. E. Machado, and E. H. Avrett, *Astrophys. J.* **360**, 715 (1990).
7. D. F. Neidig, S. R. Kane, M. Hrovat, and H. Grosser, *Bull. Amer. Astron. Soc.* **21**, 846 (1989).
8. D. F. Neidig, A. L. Kiplinger, H. S. Cohl, and P. H. Wiborg, *Astrophys. J.*, in press (1992).
9. Z. Svestka, *Adv. Astron. Astrophys.* **3**, 119 (1965).

For

I

d

lon

By

Distribution/

Availability Codes

Dist

Avail and/or
Special

DTIC QUALITY INSPECTED 8

A-1/20